Atmos. Chem. Phys. Discuss., 13, 5687–5728, 2013
www.atmos-chem-phys-discuss.net/13/5687/2013/
doi:10.5194/acpd-13-5687-2013

Atmospheric Chemistry and Physics Discussions

Atmospheric mercury over sea ice during the OASIS-2009 campaign

A. Steffen[1,2], J. Bottenheim[1], A. Cole[1], T. A. Douglas[3], R. Ebinghaus[2,4], U. Friess[5], S. Netcheva[1], S. Nghiem[6], H. Sihler[5], and R. Staebler[1]

[1]Environment Canada, Science and Technology Branch, 4905 Dufferin St., Toronto, Ontario, M3H 5T4, Canada
[2]Leuphana University Lüneburg, Institute of Sustainable & Environmental Chemistry (ISEC), Scharnhorststr. 1/13, 21335 Lüneburg, Germany
[3]US Army Cold Regions Research & Engineering Laboratory, Fort Wainwright, Alaska 99703, USA
[4]Helmholtz-Zentrum Geesthacht, Institute of Coastal Research, Department for Environmental Chemistry, Max-Planck-Str. 1, 21502 Geesthacht, Germany
[5]Institute of Environmental Physics, University of Heidelberg, Im Neuenheimer Feld 229, 69120 Heidelberg, Germany
[6]Jet Propulsion Laboratory, California Institute of Technology, Pasadena, California, USA

Received: 3 February 2013 – Accepted: 7 February 2013 – Published: 4 March 2013

Correspondence to: A. Steffen (alexandra.steffen@ec.gc.ca)

Published by Copernicus Publications on behalf of the European Geosciences Union.

Abstract

Measurements of gaseous elemental mercury (GEM), reactive gaseous mercury (RGM) and particulate mercury (PHg) were collected on sea ice near open leads in the Beaufort Sea near Barrow, Alaska in March 2009 as part of the Ocean-Atmosphere-Sea Ice-Snowpack (OASIS) International Polar Year Program. These results represent the first atmospheric mercury speciation measurements collected on the sea ice. Concentrations of PHg over the sea ice averaged 393.5 $pg\,m^{-3}$ (range 47.1–900.1 $pg\,m^{-3}$) during the two week long study. RGM concentrations averaged 30.1 $pg\,m^{-3}$ (range 3.5–105.4 $pg\,m^{-3}$). The mean GEM concentration of 0.59 $ng\,m^{-3}$ during the entire study (range 0.01–1.51 $ng\,m^{-3}$) was depleted compared to annual Arctic ambient boundary layer concentrations. It was shown that when ozone (O_3) and bromine oxide (BrO) chemistry are active there is a linear relationship between GEM, PHg and O_3 but there was no correlation between RGM and O_3. There was a linear relationship between RGM and BrO and our results suggest that the origin and age of air masses play a role in determining this relationship. These results were the first direct measurements of these atmospheric components over the sea ice. For the first time, GEM was measured simultaneously over the tundra and the sea ice. The results show a significant difference in the magnitude of the emission of GEM from the two locations where significantly higher emission occurs over the tundra. Elevated chloride levels in snow over sea ice are believed to be the cause of lower GEM emissions over the sea ice because chloride has been shown to suppress photoreduction processes of Hg(II) to Hg(0) (GEM) in snow. These results are important because while GEM is emitted after depletion events on snow inland, less GEM is emitted over sea ice. Since the snow pack on sea ice retains more mercury than inland snow current models of the Arctic mercury cycle, which are based predominantly on land based measurements, may greatly underestimate atmospheric deposition fluxes. Land based measurements of atmospheric mercury deposition may also underestimate the impacts of sea ice changes on the mercury cycle in the Arctic. The findings reported in this study improve the current

ACPD
13, 5687–5728, 2013

understanding of mercury cycling in the changing Arctic. The predicted changes in sea ice conditions and a more saline snow pack in the Arctic could lead to even greater retention of atmospherically deposited mercury in the future. This could severely impact the amount of mercury entering the Arctic Ocean and coastal ecosystems.

1 Introduction

Mercury is a toxic pollutant found in all compartments of the environment. Its presence in the environment derives from both natural and anthropogenic sources. At elevated levels, in a methylated form, mercury can be a neurotoxin to wildlife and humans. Thus, understanding how it enters and is distributed within ecosystems is crucial for the protection of the environment. The Arctic is vulnerable to mercury pollution and much has been published on its cycling in this unique environment (Steffen et al., 2008; Douglas et al., 2012b; Stern et al., 2012). The average northern hemispheric gaseous elemental mercury (GEM) concentration has been reported to be approximately 1.7 $\mathrm{ng\,m^{-3}}$ in 2003 (Slemr et al., 2003) with more recent reports showing lower concentrations at some sites (Ebinghaus et al., 2011; Slemr et al., 2011). The mean GEM concentration for the high Arctic site Alert has been reported to be 1.54 and 1.39 $\mathrm{ng\,m^{-3}}$ annually and in the spring, respectively (Steffen et al., 2005).

The Arctic atmosphere plays a key role in processes controlling mercury deposition to snow and ice surfaces. In the spring, through a series of photochemically initiated reactions, mercury is oxidized from its predominant elemental form Hg(0) in the air to an inorganic Hg(II) species. This process is called an atmospheric mercury depletion event (AMDE). These reactions have been shown to be in direct relation to the depletion of ozone (O_3) in the Arctic which is initiated by sea salts, sunlight, and cold temperatures (Simpson et al., 2007; Steffen et al., 2008). These reports suggest that Hg(0) or GEM is converted to species known as reactive gaseous mercury (RGM) and particulate mercury (PHg). RGM and PHg are operationally defined as mercury that adsorbs to a KCl denuder (gas phase) and mercury that is collected on particles < 2.5 µm, respectively.

ACPD
13, 5687–5728, 2013

GEM, RGM and PHg are collectively termed speciated mercury. Concentrations of RGM and PHg vary by location and season, however, there are significant differences reported between temperate background sites and high Arctic sites. Background concentrations for several North American studies have been reported to range between approximately 2–25 and 1–54 $pg\,m^{-3}$ for RGM and PHg, respectively (Poissant et al., 2005; Lynam and Keeler, 2006; Lyman and Gustin, 2008). In contrast, in the high Arctic at Alert, concentrations of RGM and PHg can range between approximately 0–340 and 0–700 $pg\,m^{-3}$ for RGM and PHg, respectively, in the spring (Cobbett et al., 2007), but are generally lower the remainder of the year. Coastal observations have reported periodic near complete conversion of Hg(0) to Hg(II) during the Arctic springtime; nevertheless, few to no data have been published from similar measurements collected on Arctic Ocean sea ice. The fate of Hg(0) and Hg(II) in the coastal environment has been the object of investigation for over a decade. It is believed that the majority of the O_3 depletion events occur over the Arctic Ocean and are meteorologically modulated to coastal measurement sites (Bottenheim and Chan, 2006). Strengthening the argument that this chemistry is initiated over the sea ice, near-complete O_3 depletion was observed over Arctic Ocean sea ice on a sailboat expedition over several months in the spring of 2008 (Bottenheim et al., 2009). Ozone lidar measurements onboard the Amundsen icebreaker observed that depleted layers were always connected to the surface and that the probability of low ozone concentrations increased with the amount of time the advected air masses had spent close to the surface in the preceding six days (Seabrook et al., 2011). Until recently, logistical and technical challenges limited our ability to collect reliable atmospheric mercury speciation (GEM, RGM and PHg) immediately over the Arctic Ocean.

Mercury has been measured in the air at coastal Arctic regions since 1995 and the results have shown that over the springtime period, when Hg(0) is converted in the air to Hg(II), there can be increased concentration of Hg in the underlying snow pack (Schroeder et al., 1998; Ebinghaus et al., 2002; Lindberg et al., 2002; Berg et al., 2003; Skov et al., 2004; Steffen et al., 2008). Some studies have shown that there are

ACPD
13, 5687–5728, 2013

mechanisms within the top of the snow pack that release some of that deposited mercury back to the air as Hg(0) which then makes it available to oxidation and deposition again (Lalonde et al., 2002; Dommergue et al., 2003; Ferrari et al., 2004; Ferrari et al., 2005; Kirk et al., 2006; Cobbett et al., 2007; Constant et al., 2007; Dommergue et al., 2007; Durnford and Dastoor, 2011; Douglas et al., 2012b). There have been reports that the level of mercury drops off in the snow pack after initial deposition and that this is the result of photo reduction processes (Poulain et al., 2004; Kirk et al., 2006; Constant et al., 2007; Sherman et al., 2010; Durnford and Dastoor, 2011). A question that remains is how much of this deposited Hg is retained by snow packs and how much is emitted. Currently, modelers use a number of roughly 50 % (Fisher et al., 2012) and 51 % (between 15 and 66.5° N) and 70 % (from 66.5° N and north) (Durnford et al., 2012) in their models for the overall Hg budgets of the Arctic system. These percent emissions are a result of the mechanisms discussed above. In a general review by Douglas et al. (2012) they estimated an overall emission to range between 60 and 80 % of deposited Hg.

As part of the March 2009 International Polar Year (IPY) Ocean-Atmosphere-Sea-Ice-Snowpack (OASIS) international campaign in Barrow, Alaska, atmospheric mercury speciation measurements and a suite of meteorological, O_3 and bromine oxide (BrO) measurements and snow pack chemical composition measurements were made over the Arctic sea ice. Other studies have collected information from platforms in the high Arctic such as icebreakers (Aspmo et al., 2006; Chaulk et al., 2011) but none have measured atmospheric mercury species directly on the ice near open leads or freshly formed sea ice. GEM measurements were made simultaneously over the tundra snow pack at an inland location for comparison. Results from this novel experiment provide new insights into the behaviour of atmospheric mercury in the Arctic Ocean environment.

ACPD
13, 5687–5728, 2013

2 Methods

2.1 Logistics and sites

The study took place near Barrow, Alaska 5 March to 4 April 2009. Most of the experiment described in this study was undertaken over the Chukchi Sea near the town of Barrow. The instrument boxes, called the "Out On The Ice" (OOTI) system, were towed on specially designed sleds behind snowmobiles onto the Arctic sea ice as close as possible to open leads. Figure 1a shows a map of the site locations and a satellite image of the sea ice conditions on 19 March. The first site (71.29° N; 156.85° W) was initially close to an open lead but the lead closed within the first day of sampling. The instruments were moved to other locations on two separate occasions on 19 March (71.36° N; 156.69° W) and 23 March (71.36° N; 156.66° W). The ice surface for the 3 sites can be described as follows: Site 1 – windblown snow over few days old frost flowers; Site 2 – snow over sea ice and Site 3 – 1 to 2 day old frost flowers (FFs). Figure 1b shows the experimental setup on the sea ice. The instrumentation was housed in 2 separate aluminium boxes (Box 1 and Box 2) that were lined with insulating foam and maintained at a temperature above freezing either through instrument-generated heat or with a heated blanket. Box 1 housed the meteorological instrumentation and the ozone instruments. Box 2 housed the mercury speciation instrumentation. All the instruments were powered using a 5-kW gas generator that was located approximately 17 m downwind of the sample inlets. Data was collected on a semi continuous basis as per the instrument methodology and data gaps occurred during site transfers or when the generator stopped working due to mechanical problems associated with the extremely cold conditions. Once the equipment was moved to a site the systems were set up as shown in the photo in Fig. 1b. The inlet of the Hg speciation system was approximately 15 cm above the snow pack or ice surface, the ozone inlets were at 1 and 10 cm from the surface, and the meteorological data were collected between 215 and 300 cm from the surface. A second mercury system was located inland with an inlet height of 85 cm from the snow surface.

ACPD
13, 5687–5728, 2013

2.2 Atmospheric mercury

Atmospheric mercury was collected using a Tekran® (Toronto, Ontario Canada) 2537A/1130/1135 mercury speciation system that measures the concentration of GEM, RGM and PHg. GEM is collected on gold traps, RGM is collected on KCl coated denuders and PHg is collected on quartz filters (2.5 µm cutoff from the impactor set up). The method has been described in detail elsewhere (Landis et al., 2002; Steffen et al., 2008). GEM samples were collected continuously on a 5 min interval (using 2 traps) while RGM/PHg were collected hourly and then analyzed over the subsequent hour. All the data were quality controlled manually following protocols used by Environment Canada (Steffen et al., 2012). Hourly averaged data was produced based on the start and end times of the Hg speciation collection (as it does not always start at the top of the hour). Thus, all ancillary data was averaged on the same start and end times as the Hg speciation for appropriate comparison of data. Measurements of GEM, RGM and PHg were made both at the OOTI and tundra sites (described above). Due to instrument problems at the tundra site, only the GEM data was used in this work.

2.3 Meteorological information

Wind speed and direction were measured using a propeller anemometer (Model 05103, R. M. Young, Traverse City, MI, USA) at 3.0 m above the surface, and a sonic anemometer (CSAT-3, Campbell Scientific, Logan, UT, USA) at 2.2 m. The orientation relative to absolute north was determined by hand-held GPS (Garmin Etrex). To determine temperatures, copper-constantan thermocouples were located inside passive radiation shields at 1.38, 0.1 m above and 0.05 m under the snow surface. A platinum resistance thermometer/relative humidity sensor (HMP45C, Campbell Scientific, Logan, UT, USA) inside a passive radiation shield was located at 2.3 m. Shortwave radiation (incoming and reflected) was monitored using silicon photovoltaic detectors (Li-190S, Li-200S, Li-Cor, Lincoln, NB, USA). Pressure was measured on site with a barometer (Model 61202V, RM Young).

ACPD
13, 5687–5728, 2013

2.4 Ozone

At the OOTI site, a Model 205 dual cell ozone monitor, manufactured by 2B Technology (Boulder, Colorado, USA), was used to measure surface level ozone. Ambient air was sampled through 1/4″ PFA tubing. A Teflon 2 µm pore sized filter was used to prevent penetration of any particles into the measuring cells. The instrument was calibrated at the beginning and end of the field campaign. Its zero was monitored for possible drift through regular zero measurements using an external ozone scrubber on the days when ozone was above a threshold of 10 ppb.

2.5 Bromine monoxide

Differential optical absorption spectroscopy (DOAS) can be used to quantify the column abundances of trace gases, such as bromine oxide (BrO), along a well-defined light path. These trace gases are determined using specific narrow band absorption structures in the ultraviolet and visible spectral regions. The BrO measurements described in this paper were collected with a long path-DOAS (LP-DOAS) instrument (Platt and Stutz, 2008). The general setup used in this study is described elsewhere (Friess et al., 2011; Liao et al., 2011). The LPDOAS telescope was located approximately 1 km inland on a building facing northwest. Two retro reflectors were installed 3623 m and 1074 m away from the telescope and provided a light path of 7246 m and 2148 m, respectively. The long light path was used under favourable meteorological conditions, whereas the short light path was used during periods of low visibility owing to fog, blowing snow or occasionally occurring mirages. Depending on meteorological conditions, spectra were recorded with integration times ranging between one and 50 s. The LPDOAS light paths were almost parallel to the coast and are therefore are used to represent the same air mass. Liao et al. (2011) concluded that BrO is often distributed homogeneously on spatial scales of up to at least 4 km, thus these measurements were correlated with the data collected at the OOTI site.

ACPD
13, 5687–5728, 2013

2.6 Snow and IC samples

Samples for major ion analyses were collected into precleaned high density polyethylene (HDPE) bags using precleaned HDPE scoops. Samples were stored frozen until arrival at the laboratory where they were allowed to melt to room temperature and were filtered through acid washed 0.45 mm polypropylene filters. Frost flower samples were diluted with 18 MW water 1000 times (by volume) prior to analysis. All sample dilutions were done in quadruplicate to assess cross sample variation in the dilution process and were determined to be repeatable within 5 % of the concentration values. Cation and anion concentrations were quantified on a Dionex ICS-3000 ion chromatograph with an AS-19 anion column and CS-12 cation column (Dionex Corporation, Sunnyvale, California) at the Cold Regions Research and Engineering Laboratory Alaska Geochemistry Laboratory. Each sample had a 10-mL injection volume. A gradient method using potassium hydroxide eluent ranged from 20 mM to 35 mM for anion analyses. Cation analyses used methane sulfonic acid eluent with a concentration of 25 mM in isocratic mode. The system flow rate was 1 mL min^{-1} and the operating temperature was 30 °C. The ion chromatograph was calibrated through repeat analysis of five calibration standards with concentrations ranging from 0.5 to 120 mg L^{-1} (within the range of analyses). Laboratory analytical anion and cation standards with values from 1 to 100 mg L^{-1} were analyzed repeatedly to verify system calibration and assess analytical precision. Based on these analyses the calculated precision for the analyses is 5 %. Peaks were identified using Chromeleon (Dionex, Sunnyvale, California) and were verified visually.

2.7 Max-DOAS

Multi Axis Differential Optical Absorption Spectroscopy (MAX-DOAS) was used to record the scattered sun light from series of viewing directions to provide information on aerosol vertical profiles (Hönninger and Platt, 2002; Frieß et al., 2004; Wagner et al., 2004) and were simulated using a radiative transfer model.

ACPD
13, 5687–5728, 2013

3 Results and discussion

3.1 Mercury measurements over the sea ice

The atmospheric mercury species measured during this campaign include gaseous elemental mercury (GEM), reactive gas phase mercury (RGM) and particulate mercury (PHg). Figure 2 shows the time series of GEM, RGM and PHg measured on the sea ice from 14–26 March 2009. Table 1a shows the descriptive statistics of this data set with a comparison to the tundra site. A GEM concentration of less than 1.063 ng m^{-3} was defined by Cole and Steffen (2011), for depletions at Alert, Canada, as an upper limit indicating that an AMDE is occurring and this limit will be used in these discussions. In this study, the GEM concentrations were below this threshold for 86 % of the total number of hourly averages with a mean concentration of 0.59 ± 0.40 ng m^{-3}. The considerable variation that is associated with AMDEs is shown by the standard deviation for all the Hg parameters reported. Average GEM concentrations in the high Arctic are expected to be lower than the northern hemispheric mean at approximately 1.54 ng m^{-3} and 1.70 ng m^{-3}, respectively (Slemr et al., 2003; Steffen et al., 2005). In the springtime at Alert, average GEM concentrations are even lower than the annual average at 1.39 ng m^{-3}. The average concentration reported on the sea ice in this study is lower than the lower springtime average from Alert. The PHg concentrations measured during in this study are high, in comparison to temperate regions (Steffen et al., 2012), showing a mean concentration of 393 ± 237 pg m^{-3} and reaching a maximum of 900 pg m^{-3}. RGM concentrations are lower than PHg with a mean concentration of 30 ± 24 pg m^{-3} and a maximum value of 105 pg m^{-3}. Figure 2 also shows the negative relationship between GEM concentration and PHg/RGM concentration during the measured time period which is commonly associated with AMDE chemistry.

On 14 March, the instruments were installed on the sea ice and subsequently moved on 19 March (22:00 UTC) and 23 March (21:00 UTC) to OOTI Sites 1–3, respectively, to assess different surfaces and proximity to open leads (Fig. 1a). The surfaces of the 3 sites ranged from a few day old frost flower field with some surface snow (new ice

ACPD
13, 5687–5728, 2013

pan), an ice pan with surface snow and an ice pan with 1–2 day old frost flowers in which we cut an open hole through the ice which quickly froze over. Frost flowers are intricate ice crystals formed from brine wicked through the sea ice that is subsequently coated with air vapour deposition (Simpson et al., 2007; Douglas et al., 2012a) and have an appearance of a flower on the surface. These three surfaces all represent highly saline surface young (nilas) sea ice. Figure 3 shows the Moderate Resolution Imaging Spectroradiometer (MODIS) satellite images of our sample locations. Bands 1, 2, and 7 from the MODIS Aqua satellite were used to identify sea ice on 14–25 March when the sky was mostly clear. The satellite images, however, show that all locations are represented dominantly by first-year sea ice (blue) and some younger sea ice (darker blue) in refrozen areas where the ice cover was fractured by ice divergence. Since the surfaces were not vastly different in salinity and had little snow cover, for this paper, we assume the surfaces are similar. From the satellite images, the interesting feature is the behaviour of the sea ice around the lead and will be discussed later.

It is thought that the chemistry that leads to AMDEs occurs in the gas phase by oxidation of GEM to RGM. Once produced, RGM can partition to particles in the air as PHg (Rutter and Schauer, 2007; Amos et al., 2012) or deposit to the surface. It has been theorized that the ratio of RGM to PHg reflects the transport distance of an air mass from where a depletion occurred and a low RGM:PHg indicates that the depletion occurred further away (Lindberg et al., 2002). Thus, if depletion events are initiated and occur over the Arctic Ocean and the measurements are collected there, it might be reasonable to expect higher RGM than PHg concentrations. However, it was found that the concentrations of PHg measured in this study were almost ten times higher than RGM over the sea ice. This was also observed in March 2008 from an icebreaker on the Beaufort Sea (as part of a Canadian funded IPY study) where the average concentration ratio of PHg:RGM approximately 10.6 (Latonas, 2010). Over the sea ice, the particle load in the air is likely the contributing factor in these elevated PHg concentrations. RGM can partition onto sea salt particles and other available surfaces (Rutter and Schauer, 2007). Both RGM and PHg have a higher dry deposition velocity (0.5

ACPD
13, 5687–5728, 2013

to 6 cm s^{-1} and 0.02 to 2 cm s^{-1}, respectively) than GEM at 0.1 to 0.4 cm s^{-1} (Zhang et al., 2009). Amos et al. (2012) showed, in their model simulation, a higher deposition of oxidized Hg at higher latitudes. They also concluded that high PHg fractions are yielded in colder air masses with high aerosol burdens. This current study supports these modelled results qualitatively, with higher PHg:RGM ratios at lower temperatures (not shown) but, due to a lack of $PM_{2.5}$ concentration data in this study, the partitioning could not be compared quantitatively. Using Max-DOAS, the position of the particle load and the thickness of the aerosol layer at the surface layer of the study site can be modeled to confirm the presence of aerosols. These estimates are not limited to the particle sizes that the mercury instrument collects PHg. The modeling results indicated small aerosol load with an extinction of 0.08 km^{-1} confined in layer 100 m thick lay over the surface on 14 and 25 March. This confirms that there is a measured concentration of particles present in the measurement area at the lower surface air. These results further suggest that, on the afternoon of 25 March, an increased aerosol load (extinction coefficient of 0.3 km^{-1}) was homogeneously distributed within 350 m from the surface and emerged following a shift of the wind direction from 225° to 25° and an increase in wind speed. This shift correlates to a shift in the PHg and RGM distribution (discussed later).

Natural sea salt, aged sea salt and other mixed particles are ubiquitous over the sea ice. In Ny-Ålesund, these particles fall into the > 0.5 µm size fraction range (Weinbruch et al., 2012). Other particle types commonly measured over the Arctic Ocean include sea salt sulphate, non sea salt sulphate, and soot/black carbon. Sea salt sulphate aerodynamic diameters have been measured in the North Atlantic greater than 0.95 µm but are lower in the springtime to a size less than 0.49 µm (Seguin et al., 2011). Non sea-salt sulphate diameter ranges between 0.49–0.95 µm (Seguin et al., 2011). Another type of suspended particle reported around the Arctic Ocean is diamond dust (Douglas et al., 2008; Domine et al., 2011). This small crystal forms in the air on clear, cold days and has a relatively large surface area onto which reactions can occur. They have been reported to have a length between 1 and 1000 µm (Ohtake et al., 1982; Walden

ACPD
13, 5687–5728, 2013

et al., 2003; Intrieri and Shupe, 2004). Douglas et al. (2008) reported high total mercury concentrations of (92–1370 ng L^{-1}) in these crystals and concluded that they are likely a source of elevated levels of Hg measured on the surface. The size of diamond dust is, for the most part, greater than the inlet (2.5 µm) however, as the ice crystals hit the impactor on the instrument, there is potential for them to shatter and be measured by the instrument (Leaitch, 2012). The contribution from diamond dust to PHg is likely minor but cannot be ruled out especially since the mercury concentration in them is so high. Thus, PHg reported here is likely capturing some of the particles described above at this location over the sea ice. Interestingly, in 2005, RGM measurements collected in Barrow inland from the sea ice (approximately 0.5 km) around the same time of year exceeded 800 pg m^{-3} at times which may suggest significantly higher RGM concentrations inland than over the sea ice (Douglas et al., 2008). Unfortunately, PHg concentrations were not measured during that study to compare with the current one. During the 2009 campaign an additional Hg speciation system was operating at the inland tundra site, however technical difficulties with the system only rendered accurate GEM concentrations and not RGM/PHg. It is likely that low temperatures and the availability of significant sea salt and sulphate aerosols, as well as ice crystals around the sea ice, enable the RGM formed in the atmosphere to adsorb onto particles are thus the cause of this predominance of PHg measured over the sea ice. This finding is significant as the majority of mass balance calculations and chemical models investigating the impact of AMDEs over the whole Arctic have relied on data collected inland or at coastal sites and not from over the ocean. Our results suggest the measurements from coastal locations may underestimate the concentration of PHg over the sea ice.

3.2 Mercury and meteorology over the sea ice

In order to understand what could influence atmospheric mercury speciation concentration data over the sea ice, several atmospheric factors were investigated. Figure 4 displays relative humidity, air temperature, wind speed and solar radiation data collected along with RGM (pink) and PHg (green) at the OOTI site. Not surprisingly, the

ACPD
13, 5687–5728, 2013

strong relationship between RGM and solar radiation indicates that RGM is derived through photochemical reactions. The results in this figure also show that PHg concentrations do not peak with solar radiation but lags behind by a few hours suggesting that this fraction of Hg is not photochemically derived. The highest peaks in PHg (15 and 22 March) are found when the air temperature is at the lowest ($< -30\,^{\circ}C$), the wind speeds are low (between 1 and 2 $m\,s^{-1}$), relative humidity is below the average and the solar radiation is in a low period. These are conditions under which ice crystals (diamond dust) form in the air providing a surface for newly formed RGM to adhere. Low temperatures also favour the partitioning of semi-volatile RGM compounds to the particle phase (Amos et al., 2012). Further, direct observations of diamond dust events were made on 21 and 22 March 2009 (Domine et al., 2011) raising the interesting hypothesis that RGM partitioning onto these crystals is the cause for the peak in PHg. The size of diamond dust is, for the most part, greater than the inlet however, as the ice crystals hit the impactor on the instrument, there is potential for them to shatter and be measured by the instrument (Leaitch, 2012). 21–22 March, the RGM and PHg data differ from the other times where they both peak during low solar radiation. The authors suggest that at the beginning of this time period an increase in RGM is reported, but as diamond dust crystals begin to form, some of this RGM associates to the crystals and are then detected as PHg. This shift could explain the near concurrent PHg and RGM peaks at this time. It should be noted that on 20/21 March fractures and leads opened up to the north of the measurement site approximately five to eight kilometres away and nilas ice formed on 22 March (Fig. 3).

The high PHg concentrations are not only due to diamond dust but can be a result of other particles present. NaCl is known to have a deliquescence point at 75 % relative humidity (Chen and Lee, 2001). Deliquescence is the point at which water vapour condenses on a particle to form an aqueous droplet. It is also thought that $-25\,^{\circ}C$ may be the approximate temperature at which the bromine chemistry begins that initiates AMDEs (Tarasick and Bottenheim, 2002; Cole and Steffen, 2010). Considering these thresholds, correlation plots of GEM, RGM and PHg below and above 75 % RH and

ACPD
13, 5687–5728, 2013

−25 °C were made (not shown). When the air temperature was below −25 °C, there was a linear correlation between GEM and PHg and air temperature (r^2 = 0.65 and 0.59, respectively). The linear relationship showed GEM decreasing when the air temperature decreases and PHg increasing when the air temperature decreases which agrees with the suggestion of the oxidation of GEM occurring below −25 °C. Interestingly, RGM was not found to correlate above an r^2 of 0.3 with either temperature bin and there were no linear correlations ($r^2 < 0.08$) between GEM and PHg at temperature above −25 °C. These results indicate that atmospheric conditions such as relative humidity and air temperature play a key role in the depletion of GEM and the presence of PHg.

Figure 5 shows the concentration of RGM and PHg, pressure and relative humidity in relation to wind direction. While it is obvious these measurements were made at locations surrounded by sea ice, the air coming from 330° to 75° is considered "from over the ocean only" and 130° to 210° has originated from the "tundra" before traveling for a short distance over sea ice (see also Fig. 1a). The air pressure data (Fig. 5b) was first plotted with wind direction and the clear groupings of air pressure and wind direction were used to define 3 air system events that presented themselves during this study (as indicated by the circles in the figure). The Hg data were then grouped as "Events 1, 2 and 3" according to these air systems. Table 2 summarizes the data shown in Fig. 5 and shows the mean (ranges) for wind direction, air pressure, PHg and RGM concentration, %RH and linear regression of PHg and RGM with ozone and BrO for the entire period and for the 3 distinct air systems/events during this study. Each data point represents hourly averaged data. The dates of these events are as follows: Event 1: 14–19 March; Event 2: 20, 21, 24 and 25 March; and Event 3: 25–26 March. The results in Fig. 5 show that when the air is from around 60° (Event 1 yellow circle – sea ice) PHg is above the total mean concentration and RGM is below. When the air is coming from 150° (Event 2 purple circle – tundra) RGM is above its total mean and PHg is just below its total mean. When the air is coming from 15° (Event 3 blue circle – sea ice) RGM is above its total mean and PHg is well below. Events 1 and 3 from over the sea

ACPD
13, 5687–5728, 2013

ice show discernable characteristics while Event 2 from over the tundra is somewhat in between. The average %RH during Events 1, 2 and 3 are below 75 %, around 75 % and above 75 %, respectively. These results show that there is a relationship between the relative concentration of either PHg or RGM and %RH. As mentioned above, the deliquescence point of NaCl is at 75 % RH which would indicate that these particles would have absorbed water, grown to where they could be more readily removed from the air at this point, are too large to be sampled (> 2.5 µm) or to a point where RGM is less likely to partition onto the sea salt and remain in the air. Interestingly, Event 3, where %RH is above 75 %, is the warmest event may also decrease the potential of RGM to partition onto particles. We suggest that when %RH is below 75 %, the PHg concentration data would include more sea salt particles in the air than when it is above 75 %.

Estimates of the distance between sample location and both the nearest refrozen ice and open water or nilas were made from the MODIS satellite images. These estimates are summarized in Table 3 and are separated into Events 1, 2 and 3. During Event 1 the sampling location was close to refrozen sea ice and that the air was coming from that direction. This close refrozen surface can reflect a strong depletion of GEM and elevated PHg (potentially a source of fresh sea salts). During Event 2 the samples were collected further from the refrozen sea ice but closer to an open lead, which could explain the increase in RGM and %RH. From full-resolution satellite images of sea ice conditions (not shown here), the 22–24 March estimates show that open leads are quite far away (18.8 to 45 km) and this is when a weaker depletion in GEM is reported (Fig. 2). On 25 March the measurement site was further from the refrozen sea ice and but a closer distance from the open water (12.5 km); however, the air mass is coming from a different direction at this time and thus the northern sea ice may not be the biggest driver in activities during this event. These results show that satellite images of sea ice conditions can help to identify depletion of mercury over the sea ice.

ACPD
13, 5687–5728, 2013

3.3 Mercury, ozone and halogens over the sea ice

The relationship between GEM and ozone (O_3) has been well documented during AMDEs in the Arctic springtime (Schroeder et al., 1998; Poissant and Pilote, 2003). The correlation suggests that a common reactant (the bromine atom) is responsible for the depletion of both. Linear regressions were performed on GEM, PHg and RGM with O_3 for the whole study period and for each Event (Tables 1 and 2). GEM and O_3 show a strong linear relationship over the sea ice ($r^2 = 0.76$). While there is a reasonable linear relationship between PHg and O_3 over the study period ($r^2 = 0.61$), the strongest relationship was reported during Event 1 ($r^2 = 0.82$). Events 2 and 3 reflect lower r^2 values that are close to the value reported for the whole study period. There is little relationship between O_3 and RGM in this data, however, RGM is a product of the bromine chemistry and its lifetime is short, thus, a strong relationship is not expected (Simpson et al., 2007). Measurements of BrO were also collected during this study and Fig. 6 shows the time series of RGM, PHg, GEM and BrO for the study and Table 2 shows the correlations of these species with BrO (for the ice data).

The data in Fig. 6 show that BrO is elevated at the beginning of a depletion event when GEM decreases and RGM/PHg increase and then BrO subsequently decreases as the event continues. The results in Table 2 show that there is little to no linear relationship between BrO and PHg but a reasonable correlation between BrO and RGM for the periods when the air originates from over the ocean (Events 1 and especially 3). RGM and BrO are both products of bromine atom chemistry which suggests that this chemistry is at play. The atmospheric conditions for Events 1 and 3 are as follows: Event 1 has high PHg, RH below 75 %, air temperature below −25 °C, good correlations between RGM and BrO, and PHg and O_3. Thus, the solid particles in the air at this time can promote Br formation that leads to RGM formation which can then partition to the available particles and produce elevated PHg concentrations. Event 3 has low PHg, RH above 75 %, air temperature above −25 °C, good correlations between RGM and BrO, and PHg and O_3. In this event, the particles are more likely droplets which lead

ACPD
13, 5687–5728, 2013

to less BrO production but enough to still produce RGM. In this case, we propose that either RGM does not adsorb to these droplets or that these droplets are not as predominant in the air. This could explain why Event 3 shows higher RGM concentrations than Events 1 and 2. The absence of a BrO/RGM correlation in Event 2 suggests that this chemistry is less evident or not occurring and that the origin of these air masses may play a role in this result. The lifetimes of both BrO and RGM are quite different which makes a direct analysis such as this challenging (BrO has a reported lifetime of 2 min, Simpson et al., 2007, and RGM, depending on the species, between 6–54 h, AMAP, 2011). However, this is the first insight into direct measurements of such species over sea ice and the complexity of the atmospheric chemistry around AMDEs. We suggest that direct measurements of in situ mercury and halogen species be undertaken during AMDEs to further understand atmospheric conditions that drive this chemistry.

3.4 Atmospheric mercury differences between sea ice and inland tundra

The difference between GEM concentrations over the sea ice and inland over the snow-covered tundra was also investigated. A summary of the GEM concentrations for the 2 locations is shown in Table 1a. The mean concentration over the tundra is higher (0.79 ± 0.56 ng m^{-3}) than those recorded over the sea ice (0.59 ± 0.40 ng m^{-3}). The lower average over the sea ice may suggest that GEM is depleted more often there than inland. The minimum concentration at both locations is the same but the maximum over the tundra is higher than over the ice (2.92 and 1.51 ng m^{-3}, respectively). A linear correlation between O_3 and GEM was made for both sites and the results are shown in Table 1a. These results show that there is a stronger linear relationship of O_3 and GEM over the sea ice than inland as reflected by r^2 values of 0.76 and 0.52, respectively. This and the higher inland mean GEM concentration can be explained by inspecting the GEM concentrations from each site together. Figure 7 shows the time series from GEM measurements inland over the tundra (grey circles) and from over the sea ice (blue circles), the solar radiation (orange dots) and the defined depletion concentration threshold (dashed grey line). This plot shows that both sites experience

ACPD
13, 5687–5728, 2013

depletion events around the same time and to the same level throughout most of the study. The slight offset observed in the data is a result of when the samples were collected.

The striking difference between these two data sets is the strong peaks of GEM at the tundra site following the end of a depletion event. GEM (and O_3) concentrations can return to background after depletion through mixing (generally from aloft), however, it has also been shown that some GEM is emitted from the surface of the snow following depletion events (Steffen et al., 2002; Poulain et al., 2004; Kirk et al., 2006) which is likely driven by photoreduction processes (Lalonde et al., 2002; Poulain et al., 2004). This study shows that there is evidence of GEM increasing to above the 1.063 ng m^{-3} mark following the strong depletions over the sea ice but not significantly (e.g. 19 and 21 March). However, the amount of GEM returning to the air over the tundra is much higher (nearly double in concentration). These results demonstrate that emission of GEM from the tundra snow pack occurs at a different magnitude than the emission recorded over the sea ice. This is the first time that this comparative observation has been directly made and measured. The instruments were run beside each other for several days and a correlation of 0.9 was found for GEM and thus the differences are not a result of instrument bias. It was also observed that after the spike in GEM concentrations at both locations the GEM is again oxidized and depleted from the air. This cycle continues throughout the study. The concentration of ozone follows GEM concentrations reasonably well at both sites (see Fig. 8). However, Fig. 8 (top) shows occurrences when spikes of GEM at the tundra site are not paralleled by ozone (24/25 and 26/27 March). These spikes in the GEM are likely due to emission of Hg from the snow surface. This is rarely observed on the sea ice (Fig. 8, bottom). The emission spikes recorded from the tundra site explain the higher average concentration reported at that location than over the sea ice. It is likely that because the emission spikes are unrelated to the O_3 chemistry that the linear relationship between O_3 and GEM over the tundra is not as strong as that over the sea ice. Further, the sea ice GEM measurements reflect more closely the impact of the atmospheric springtime depletion

ACPD
13, 5687–5728, 2013

chemistry. In addition, modeling of mercury in the cryosphere suggests that PHg will be retained in the snow pack more than GEM and RGM (Durnford and Dastoor, 2011) and is also reflected in the results reported here.

The explanation for the absence of GEM spikes over the sea ice is likely to be the presence of large quantities of NaCl over the ocean. It was suggested by Poulain et al. (2004) and Lehnherr and St. Louis (2009) that the photoreduction of oxidized mercury is suppressed by the presence of chloride. To investigate this further, snow samples from over the sea ice and around the land tundra site were collected and analyzed for major ions and total mercury. The samples were collected randomly over the study period and thus were averaged for overall concentrations rather than reported daily. The overall results showed that the average concentration of mercury in the surface snow over land and sea ice were $66 \pm 30\,\mathrm{pg\,L^{-1}}$ and $75 \pm 47\,\mathrm{ng\,L^{-1}}$, respectively. These results indicate that there is generally more Hg in snow over the ice than over the tundra which is as expected, since the Hg in tundra snow is re-emitted, and the Hg over ice is not. Samples of brine around sea ice measurement sites averaged Hg concentrations of $83.1 \pm 58.4\,\mathrm{ng\,L^{-1}}$ and samples of frost flowers averaged $93.7 \pm 60.8\,\mathrm{ng\,L^{-1}}$. While the uncertainties show that these concentrations are not statistically different, they do follow the pattern of previously reported results (Douglas et al., 2008). These latter results show that the concentration of mercury in brine and frost flowers is higher than that in the snow. Major ion concentrations in snow over the sea ice and over the land were also measured. Results showed that the chloride concentrations were six times higher over the sea ice than the land snow and the bromide concentrations were double over the sea ice than land. The presence of higher concentration of chloride in the snow over the sea ice agrees well with the hypothesis that the lower spikes reported in the emission of Hg(0) over the sea ice in comparison to over the land may result from the suppression of photoreduction processes of Hg(II) to Hg(0) by the presence of chloride. These results are significant as it shows that even though Hg(0) tends to be re-emitted after depletion events on snow inland, less (or none at all) Hg(0) is re-emitted over the sea ice. Thus, we conclude that the sea ice snow retains more mercury than surface

ACPD
13, 5687–5728, 2013

snow inland. This result needs to be factored into the current models predicting the impacts of sea ice changes on the mercury cycle over the Arctic Ocean.

4 Conclusions

In March 2009, measurements of GEM, RGM and PHg were collected near new sea ice and open leads and fractures in the Chukchi/Beaufort Sea near Barrow, Alaska as part of the OASIS International Polar Year Program. These results represent the first atmospheric mercury speciation measurements collected and reported on the sea ice. Ozone, bromine oxide and a suite of meteorological parameters were reported and demonstrated the role of the atmosphere in the cycling of mercury over the sea ice. Results found high levels of PHg associated with different types of particles and low air temperatures over the sea ice. The average PHg concentration over the sea ice was 393.5 $\mathrm{pg\,m^{-3}}$ (ranging from 47.1 to 900.1 $\mathrm{pg\,m^{-3}}$). RGM concentrations were also elevated and averaged 30.1 $\mathrm{pg\,m^{-3}}$ (ranging from 3.5 to 105.4 $\mathrm{pg\,m^{-3}}$) but were not as high as PHg. GEM was reported to average 0.59 $\mathrm{ng\,m^{-3}}$ (ranging from 0.01 to 1.51 $\mathrm{ng\,m^{-3}}$). Sea salts and ice crystals around the sea ice provide surfaces to which RGM, created through AMDEs, can adsorb.

Atmospheric conditions (relative humidity, wind speed and air temperature) in which these particles were observed were found to have impacts on the cycling of mercury over the sea ice. These results showed that the conditions over the sea ice are favourable for enhanced deposition of PHg. This finding is significant as the majority of mass balance calculations and models investigating the impact of AMDEs over the whole Arctic have relied on data collected inland or at coastal sites and not from measurements made over the ocean. These results suggest the measurements from coastal locations may underestimate the concentration of PHg over the sea ice.

Three distinct events occurred during the study that reflected different air masses and allowed for the conditions under which the active chemistry could be studied. It was shown that, when O_3 and BrO chemistry is active, there is a linear relationship

ACPD
13, 5687–5728, 2013

between GEM, PHg and O_3 and between RGM and BrO. When these relationships fail, it was concluded that the origin of the air mass must play a role in the AMDEs. These results were the first direct measurements over the sea ice of Hg and BrO and O_3 and demonstrate the complexity of the atmospheric chemistry associated with AMDEs. Direct in-situ mercury speciation and halogen measurements during AMDEs are recommended to more clearly derive the chemical and physical processes in real life situations.

For the first time, GEM was reported simultaneously at sites over the tundra and the nearby sea ice. A comparison of the results shows a significant difference in the magnitude of the emission of GEM once AMDEs have ceased from the two locations. Higher chloride concentrations in the snow over the sea ice are the most likely cause of lower GEM emission over the sea ice. This is caused from the suppression of photoreduction processes of Hg(II) to Hg(0) by the presence of chloride. These results are significant as it shows that even though Hg(0) tends to be emitted from the snow pack after depletion events inland, less Hg(0) is emitted from the snow pack on sea ice. Thus, we conclude that the sea ice snow retains more mercury than surface snow inland. This result needs to be factored into modeling efforts predicting the impacts of sea ice changes on the mercury cycle over the Arctic Ocean.

The findings reported in this study have major implications for mercury cycle in a changing Arctic. The sea ice on the Arctic Ocean is rapidly moving toward a greater fraction of thinner, more dynamic first year ice with the following characteristics: more open leads, enhanced sea salt particle formation, more new ice formation, more frost flowers, more brine wicking to the ice surface (Serreze et al., 2007; Stroeve et al., 2007; Rothrock et al., 2008; Shepson et al., 2003; Rigor and Wallace, 2004; Nghiem et al., 2006; Maslanik et al., 2007; Douglas et al., 2012). As a consequence, the future Arctic Ocean sea ice and snow pack regime are expected to be more halogen and sea salt rich and this could have major implications on the deposition and ultimate fate of Hg in the Arctic.

ACPD
13, 5687–5728, 2013

Mercury chemistry is related to bromine chemistry and if that is increased by changing Arctic sea ice and atmospheric conditions we will have an increase in AMDEs. The most significant finding from our work is that Hg(II) deposited from AMDEs is less readily photoreduced back to the atmosphere in the presence of sea salts. This can be projected that the more sea salt on the surface in the Arctic Ocean (and potentially inland), the more deposited mercury will be retained. Thus, the present (and future) Arctic Ocean is likely a larger sink for atmospherically deposited mercury than has been previously reported through field and modeling activities. Any potential for snow enriched in sea salts to move from the sea ice to the land in coastal environments will have higher mercury retention and thus a stronger impact of AMDEs on the coastal ecosystems.

Acknowledgement. The authors would like to thank Environment Canada and the Canadian International Polar Year Program for funding this project. T. Douglas acknowledges instrumentation support from the US Army Cold Regions Research and Engineering Laboratory and financial support from the US National Science Foundation and the US National Aeronautics and Space Administration. Logistical support in Barrow was provided by the Barrow Arctic Science Consortium. The authors acknowledge icebreaker Hg data referred to in the text collected during the Circumpolar Flaw Lead System Study as part of the Canadian International Polar Year Program. The authors thank Patrick Lee for field technical support and Julie Narayan for data analysis support. The research carried out at the Jet Propulsion Laboratory, California Institute of Technology, was supported by the National Aeronautics and Space Administration (NASA) Cryospheric Sciences Program.

References

AMAP: Amap assessment 2011: Mercury in the arctic, Arctic Monitoring and Assessment Programme (AMAP), Oslo, Norwayxiv, 193 pp., 2011.

Amos, H. M., Jacob, D. J., Holmes, C. D., Fisher, J. A., Wang, Q., Yantosca, R. M., Corbitt, E. S., Galarneau, E., Rutter, A. P., Gustin, M. S., Steffen, A., Schauer, J. J., Graydon, J. A., Louis, V. L. St., Talbot, R. W., Edgerton, E. S., Zhang, Y., and Sunderland, E. M.:

ACPD
13, 5687–5728, 2013

Gas-particle partitioning of atmospheric Hg(II) and its effect on global mercury deposition, Atmos. Chem. Phys., 12, 591–603, doi:10.5194/acp-12-591-2012, 2012.
Aspmo, K., Temme, C., Berg, T., Ferrari, C., Gauchard, P.-A., Fain, P.-A., and Wibetoe, G.: Mercury in the atmosphere, snow and melt water ponds in the north atlantic ocean during arctic summer, Environ. Sci. Technol., 40, 4083–4089, 2006.
Berg, T., Sommar, J., Wängberg, I., Gårdfeldt, K., Munthe, J., and Schroeder, W. H.: Arctic mercury depletion events at two elevations as observed at the zeppelin station and dirigibile Italia, Ny-Ålesund, Spring 2002, J. Phys. IV, 107, 151–154, 2003.
Bottenheim, J. and Chan, H. M.: A trajectory study into the origin of spring time arctic boundary layer ozone depletion, J. Geophys. Res., 111, D19301, doi:10.1029/2006JD007055, 2006.
Bottenheim, J. W., Netcheva, S., Morin, S., and Nghiem, S. V.: Ozone in the boundary layer air over the Arctic Ocean: measurements during the TARA transpolar drift 2006–2008, Atmos. Chem. Phys., 9, 4545–4557, doi:10.5194/acp-9-4545-2009, 2009.
Chaulk, A., Stern, G. A., Arnstrong, D., Barber, D. G., and Wang, F.: Mercury distribution and transport across the ocean-sea-ice-atmosphere interface on the arctic ocean, Environ. Sci. Technol., 45, 1866–1872, doi:10.1021/es103434c, 2011.
Chen, Y. Y. and Lee, W. M.: The effect of surfactants on deliquescence of sodium chloride, J. Environ. Sci. Health A, 36, 229–242, 2001.
Cobbett, F. D., Steffen, A., Lawson, G., and Van Heyst, B. J.: Gem fluxes and atmospheric mercury concentrations (GEM, RGM and HGP) in the Canadian Arctic at Alert, Nunavut, Canada (February–June 2005), Atmos. Environ., 41, 6527–6543, 2007.
Cole, A. S. and Steffen, A.: Trends in long-term gaseous mercury observations in the Arctic and effects of temperature and other atmospheric conditions, Atmos. Chem. Phys., 10, 4661–4672, doi:10.5194/acp-10-4661-2010, 2010.
Constant, P., Poissant, L., Villemur, R., and Lean, D.: Fate of mercury and methylmercury within the snow cover at Whapmagoostui-Kuujjuarapik (Québec, Canada), J. Geophys. Res.-Atmos., 112, D08309, doi:10.1029/2006JD007961, 2007.
Domine, F., Gallet, J.-C., Barret, M., Houdier, S., Voisin, D., Douglas, T. A., Blum, J., Beine, H. J., Anastasio, C., and Breon, F.-M.: The specific surface area and chemical composition of diamond dust near Barrow, Alaska, J. Geophys. Res., 116, D00R06, doi:10.1029/2011JD016162, 2011.

ACPD
13, 5687–5728, 2013

Dommergue, A., Ferrari, C. P., Gauchard, P.-A., Boutron, C. F., Poissant, L., Pilote, M., Jitaru, P., and Adams, F.: The fate of mercury species in a sub-arctic snow-pack during snowmelt, Geophys. Res. Lett., 30, 1621, doi:10.1029/2003GL017308, 2003.

Dommergue, A., Bahlmann, E., Ferrara, R., and Boutron, C. F.: Laboratory simulation of Hg_0 emissions from a snowpack, Anal. Bioanal. Chem., 388, 319–327, 2007.

Douglas, T., Sturm, M., Simpson, W., Blum, J., Alvarez-Aviles, L., Keeler, G., Perovich, D., Biswas, A., and Johnson, K.: The influence of snow and ice crystal formation and accumulation on mercury deposition to the Arctic, Environ. Sci. Technol., 42, 1542–1551, 2008.

Douglas, T. A., Domine, F., Barret, M., Anastasio, C., Beine, H. J., Bottenheim, J., Grannas, A., Houdier, S., Netcheva, S., Rowland, G., Staebler, R., and Steffen, A.: Frost flowers growing in the arctic ocean-atmosphere-sea ice-snow interface: 1. Chemical composition, J. Geophys. Res. D: Atmos., 117, D00R09, doi:10.1029/2011JD016460, 2012a.

Douglas, T. A., Loseto, L. L., Macdonald, R. W., Outridge, P. M., Dommergue, A., Poulain, A., Amyot, M., Barkay, T., Berg, T., Chetelat, J., Constant, P., Evans, M., Ferrari, C. P., Gantner, N., Johnson, M. S., Kirk, J. L., Kroer, N., Larose, C., Lean, D., Nielsen, T. G., Poissant, L., Rignerud, S., Skov, H., Sorensen, S., Wang, F., Wilson, S., and Zdanowicz, C.: The fate of mercury in arctic terrestrial and aquatic ecosystems, a review, Environ. Chem., 9, 321–355, doi:10.1071/EN11140, 2012b.

Durnford, D. and Dastoor, A.: The behavior of mercury in the cryosphere: a review of what we know from observations, J. Geophys. Res. D: Atmos., 116, D06305, doi:10.1029/2010JD014809, 2011.

Durnford, D., Dastoor, A., Ryzhkov, A., Poissant, L., Pilote, M., and Figueras-Nieto, D.: How relevant is the deposition of mercury onto snowpacks? – Part 2: A modeling study, Atmos. Chem. Phys., 12, 9251–9274, doi:10.5194/acp-12-9251-2012, 2012.

Ebinghaus, R., Kock, H. H., Temme, C., Einax, J. W., Lowe, A. G., Richter, A., Burrows, J. P., and Schroeder, W. H.: Antarctic springtime depletion of atmospheric mercury, Environ. Sci. Technol., 36, 1238–1244, 2002.

Ebinghaus, R., Jennings, S. G., Kock, H. H., Derwant, R. G., Manning, A. J., and Spain, T. G.: Decreasing trends in total gaseous mercury in baseline air at Mace Head, Ireland from 1996–2009, Atmos. Environ., 159, 1577–1583, 2011.

Ferrari, C. P., Dommergue, A., and Boutron, C. F.: Profiles of mercury in the snow pack at Station Nord, Greenland shortly after polar sunrise, Geophys. Res. Lett., 31, L03401, doi:10.1029/2003GL018961, 2004.

ACPD
13, 5687–5728, 2013

Ferrari, C. P., Gauchard, P. A., Dommergue, A., Magand, O., Nagorski, S., Boutron, C. F., Temme, C., Bahlmann, E., Ebinghaus, R., Steffen, A., Banic, C., Aspmo, K., Berg, T., Planchon, F., and Barbante, C.: Snow to air exchange of mercury in an arctic seasonal snow pack in Ny-Alesund, Svalbard, Atmos. Environ., 39, 7633–7645, 2005.

Fisher, J. A., Jacob, D. J., Soerensen, A. L., Amos, H. M., Steffen, A., and Sunderland, E. M.: Riverine source of artic ocean mercury inferred from atmopsheric observations, Nature Geosci., 5, 499–504, NGO01478, doi:10.1038/NGEO1478, 2012.

Frieß, U., Monks, P. S., Remedios, J. J., Rozanov, A., Sinreich, R., Wagner, T., and Platt, U.: MAX-DOAS O_4 measurements: a new technique to derive information on atmospheric aerosols: 2. Modeling studies, J. Geophys. Res., 111, D14203, doi:10.1029/2005JD006618, 2004.

Friess, U., Sihler, H., Sander, R., Poehler, D., Yilmaz, S., and Platt, U.: The vertical distribution of bro and aerosols in the Arctic: measurements by active and passive differential optical absorption spectroscopy, J. Geophys. Res., 116, D00R04, doi:10.1029/2011JD015938, 2011.

Hönninger, G. and Platt, U.: Observations of bro and its vertical distribution during surface ozone depletion at alert, Atmos. Environ., 36, 2481–2489, 2002.

Intrieri, J. M. and Shupe, M. D.: Characteristics and radiative effects of diamond dust over the western Arctic Ocean region, J. Climatol., 17, 2953–2960, 2004.

Kirk, J. L., St. Louis, V. L., and Sharp, M. J.: Rapid reduction and reemission of mercury deposited into snow packs during atmospheric mercury depletion events at Churchill, Manitoba, Canada, Environ. Sci. Technol., 40, 7590–7596, 2006.

Lalonde, J. D., Poulain, A. J., and Amyot, M.: The role of mercury redox reactions in snow on snow-to-air mercury transfer, Environ. Sci. Technol., 36, 174–178, 2002.

Landis, M., Stevens, R. K., Schaedlich, F., and Prestbo, E. M.: Development and characterization of an annular denuder methodology for the measurement of divalent inorganic reactive gaseous mercury in ambient air, Environ. Sci. Technol., 36, 3000–3009, 2002.

Latonas, J.: Measurements of atmospheric mercury, dissolved gaseous mercury, and evasional fluxes in the Amundsen Gulf: the role of the sea-ice environment masters, Department of Environment and Geography, University of Manitoba, Winnipeg, 165 pp., 2010.

Leaitch, R.: Personal communication, 2012.

Liao, J., Sihler, H., Huey, L. G., Neuman, J. A., Tanner, D. J., Friess, U., Playy, U., Flocke, F. M., Orlando, J. J., Shepson, P. B., Beine, H. J., Weinheimer, A. J., Sjostedt, S. J., Nowak, J. B., Knapp, D. J., Staebler, R. M., Zheng, W., Sander, R., Hall, S. R., and Ullmann, K.:

ACPD
13, 5687–5728, 2013

A comparison of arctic bro measurements by chemical ionization mass spectrometry and long path-differential optical absorption spectroscopy, J. Geophys. Res., 116, D00R02, doi:10.1029/2010JD014788, 2011.
Lindberg, S. E., Brooks, S., Lin, C.-J., Scott, K. J., Landis, M. S., Stevens, R. K., Goodsite, M., and Richter, A.: Dynamic oxidation of gaseous mercury in the arctic troposphere at polar sunrise, Environ. Sci. Technol., 36, 1245–1256, 2002.
Lyman, S. N. and Gustin, M. S.: Speciation of atmospheric mercury at two sites in Northern Nevada, USA, Atmos. Environ., 42, 927–939, 2008.
Lynam, M. M. and Keeler, G. J.: Source-receptor relationships for atmospheric mercury in urban Detroit, Michigan, Atmos. Environ., 40, 3144–3155, 2006.
Ohtake, T., Jayaweera, K., and Sakurai, K.-I.: Observation of ice crystal formation in lower arctic atmosphere, J. Atmos. Sci., 39, 2898–2904, 1982.
Platt, U. and Stutz, J.: Differential Optical Absorption Spectroscopy: Principles and Applications, Springer, Heidelberg, Germany, 2008.
Poissant, L. and Pilote, M.: Time series analysis of atmospheric mercury in Kuujjuarapik/Whapmagoostui (Quebec), J. Phys. IV, 107, 1079–1082, 2003.
Poissant, L., Pilote, M., Beauvais, C., Constant, P., and Zhang, H. H.: A year of continuous measurements of three atmospheric mercury species (gem, rgm and hgp) in southern Quebec, Canada, Atmos. Environ., 39, 1275–1287, 2005.
Poulain, A. J., Lalonde, J. D., Amyot, J. D., Shead, J. A., Raofie, F., and Ariya, P. A.: Redox transformations of mercury in an arctic snowpack at springtime, Atmos. Environ., 38, 6763–6774, 2004.
Rutter, A. P. and Schauer, J. J.: The impact of aerosol composition on the particle to gas partitioning of reactive mercury, Environ. Sci. Technol., 41, 3934–3939, 2007.
Schroeder, W. H., Anlauf, K. G., Barrie, L. A., Lu, J. Y., Steffen, A., Schneeberger, D. R., and Berg, T.: Arctic springtime depletion of mercury, Nature, 394, 331–332, 1998.
Seabrook, J. A., Whiteway, J., Staebler, R. M., Bottenheim, J. W., Komguem, L., Gray, L. H., Barber, D., and Asplin, M.: Lidar measurements of arctic boundary layer ozone depletion events over the frozen ocean, J. Geophys. Res. D: Atmos., 116, D00S02, doi:10.1029/2011JD015938, 2011.
Seguin, A. M., Norman, A.-L., Eaton, S., and Wadleigh, M.: Seaonality in size segregated biogenic, anthorpogenic and sea salt sulfate aerosols over the North Atlantic, Atmos. Environ., 45, 6947–6954, 2011.

ACPD
13, 5687–5728, 2013

Sherman, L. S., Blum, J. D., Johnson, K. P., Keeler, G. J., Barres, J. A., and Douglas, T. A.: Mass-independent fractionation of mercury isotopes in arctic snow driven by sunlight, Nature Geosci., 3, 173–177, doi:10.1038/ngeo758, 2010.

Simpson, W. R., von Glasow, R., Riedel, K., Anderson, P., Ariya, P., Bottenheim, J., Burrows, J., Carpenter, L. J., Frieß, U., Goodsite, M. E., Heard, D., Hutterli, M., Jacobi, H.-W., Kaleschke, L., Neff, B., Plane, J., Platt, U., Richter, A., Roscoe, H., Sander, R., Shepson, P., Sodeau, J., Steffen, A., Wagner, T., and Wolff, E.: Halogens and their role in polar boundary-layer ozone depletion, Atmos. Chem. Phys., 7, 4375–4418, doi:10.5194/acp-7-4375-2007, 2007.

Skov, H., Christensen, J. H., Heidam, N. Z., Jensen, B., Wahlin, P., and Geernaert, G.: Fate of elemental mercury in the artcic during atmospheric depletion episodes and the load of atmospheric mercury to the arctic, Environ. Sci. Technol., 38, 2373–2382, 2004.

Slemr, F., Brunke, E., Ebinghaus, R., Temme, C., Munthe, J., Wängberg, I., Schroeder, W. H., Steffen, A., and Berg, T.: Worldwide trend of atmospheric mercury since 1977, Geophys. Res. Lett., 30, 23–21, 2003.

Slemr, F., Brunke, E.-G., Ebinghaus, R., and Kuss, J.: Worldwide trend of atmospheric mercury since 1995, Atmos. Chem. Phys., 11, 4779–4787, doi:10.5194/acp-11-4779-2011, 2011.

Steffen, A., Schroeder, W. H., Bottenheim, J., Narayan, J., and Fuentes, J. D.: Atmospheric mercury concentrations: Measurements and profiles near snow and ice surfaces in the canadian arctic during alert 2000, Atmos. Environ., 36, 2653–2661, 2002.

Steffen, A., Schroeder, W. H., Macdonald, R., Poissant, L., and Konoplev, A.: Mercury in the arctic atmosphere: an analysis of eight years of measurements of gem at Alert (Canada) and a comparison with observations at Amderma (Russia) and Kuujjuarapik (Canada), Sci. Total Environ., 342, 185–198, 2005.

Steffen, A., Douglas, T., Amyot, M., Ariya, P., Aspmo, K., Berg, T., Bottenheim, J., Brooks, S., Cobbett, F., Dastoor, A., Dommergue, A., Ebinghaus, R., Ferrari, C., Gardfeldt, K., Goodsite, M. E., Lean, D., Poulain, A. J., Scherz, C., Skov, H., Sommar, J., and Temme, C.: A synthesis of atmospheric mercury depletion event chemistry in the atmosphere and snow, Atmos. Chem. Phys., 8, 1445–1482, doi:10.5194/acp-8-1445-2008, 2008.

Steffen, A., Scherz, T., Olson, M. L., Gay, D. A., and Blanchard, P.: A comparison of data quality control protocols for atmospheric mercury speciation measurements, J. Environ. Monit., 14, 752–765, doi:10.1039/c2em10735j, 2012.

ACPD
13, 5687–5728, 2013

Stern, G., Macdonald, R. W., Outridge, P. M., Wilson, S., Chetelat, J., Cole, A., Hintlemann, H., Loseto, L. L., Steffen, A., Wang, F., and Zdanowicz, C.: How does climate change influence arctic mercury?, Sci. Total Environ., 414, 22–42, 2012.

Tarasick, D. W. and Bottenheim, J. W.: Surface ozone depletion episodes in the Arctic and Antarctic from historical ozonesonde records, Atmos. Chem. Phys., 2, 197–205, doi:10.5194/acp-2-197-2002, 2002.

Wagner, T., Dix, B., von Friedeburg, C., Frieß, U., Sanghavi, S., Sinreich, R., and Platt, U.: Max-doas o4 measurements: a new technique to derive information on atmospheric aerosols-principles and information content, J. Geophys. Res., 109, D22205, doi:10.1029/2004JD004904, 2004.

Walden, V. P., Warren, S. G., and Tuttle, E.: Atmospheric ice crystals over the anrarctic plateau in winter, J. Appl. Meteorol., 42, 1391–1405, 2003.

Weinbruch, S., Wiesemann, D., Ebert, M., Schütze, K., Kallenborn, R., and Ström, J.: Chemical composition and sources of aerosol particles at Zeppelin Mountain (Ny Ålesund, Svalbard): an electron microscopy study, Atmos. Environ., 49, 142–150, 2012.

Zhang, L., Wright, L. P., and Blanchard, P.: A review of current knowledge concerning dry deposition of atmospheric mercury, Atmos. Environ., 43, 5853–5864, 2009.

ACPD
13, 5687–5728, 2013

Table 1a. Mercury concentration data descriptive statistics from measurements over the sea ice and tundra.

	GEM Ice ($ng\,m^{-3}$)	PHg Ice ($pg\,m^{-3}$)	RGM Ice ($pg\,m^{-3}$)	GEM Tundra ($ng\,m^{-3}$)
Mean	0.59	393.49	30.10	0.79
Median	0.53	332.76	25.04	0.75
Std. Dev	0.40	236.74	23.69	0.56
Max	1.51	900.11	105.40	2.92
Min	0.01	47.09	3.52	0.00
R^2 O_3 v Hg	0.76	0.61	0.10	0.52

ACPD
13, 5687–5728, 2013

Table 1b. Meteorology around PHg spikes over sea ice (average over time period of elevated PHg).

Date	PHg ($pg\,m^{-3}$)	Wind speed ($m\,s^{-1}$)	Air temperature (°C)	Relative humidity (%)	Radiation average
15 Mar 01:50 to 15:50	861	2.1	−32.1	66.1	25.8
21 Mar 01:00 to 17:00	595	1.7	−32.2	68	49.4
23 Mar 03:35 to 17:35	479	1.6	−23.8	77.6	15.3

ACPD
13, 5687–5728, 2013

Table 2. Summary information for data collected over the sea ice for the total study period and Events 1, 2 and 3.

	Units	Total	Event 1 (yellow)	Event 2 (purple)	Event 3 (blue)
Dates		14–26 Mar	14–19 Mar	20, 21, 24 Mar	25–26 Mar
Wind direction Centre (range)	Degree	210–330	60 (30–90)	150 (120–180)	15 (0–30)
Air pressure Mean (range)	Torr	1035 (1012–1042)	1035 (1026–1041)	1038 (1035–1042)	1019 (1012–1035)
PHg concentration Mean (range)	pg m^{-3}	393.5 (47.1–900.1)	**449.8** (123.1–898.9)	**367.4** (47.1–900.1)	**255.5** (140.2–319.6)
RGM concentration Mean (range)	pg m^{-3}	30.1 (3.5–105.4)	**18.3** (3.5–71.8)	**39.4** (12.8–105.4)	**42.9** (7.4–95.7)
% relative humidity Mean (range)	percent	74.8 (61.3–82.3)	71.5 (61.7–78.7)	75.9 (64.2–82.3)	80.7 (78.2–81.9)
R^2 with ozone PHg/RGM	n/a	0.61/0.10	0.82/0.01	0.63/0.19	0.58/0.29
R^2 with BrO GEM/PHg/RGM	n/a	0.48/0.1/0.36	0.58/0.08/0.74	0.04/0.14/0.01	0.03/0.03/0.37
Number of data points	n/a	96–101	37–44	42–50	10–12

ACPD
13, 5687–5728, 2013

Table 3. Estimated distances from the sampling locations on the sea ice to the nearest refrozen sea ice and nearest open water or nilas according to date and Event.

Date	Distance to nearest refrozen sea ice (km)	Distance to nearest open water or nilas (km)	Corresponding Event
14 Mar	1.4	11.0	1
15 Mar	1.2	7.0	1
16 Mar	1.8	9.0	1
20 Mar	4.4	5.4	2
21 Mar	5.0	8.5	2
22 Mar	5.8	45.0	
23 Mar	6.7	29.6	
24 Mar	6.8	18.8	2
25 Mar	6.3	12.5	3

ACPD
13, 5687–5728, 2013

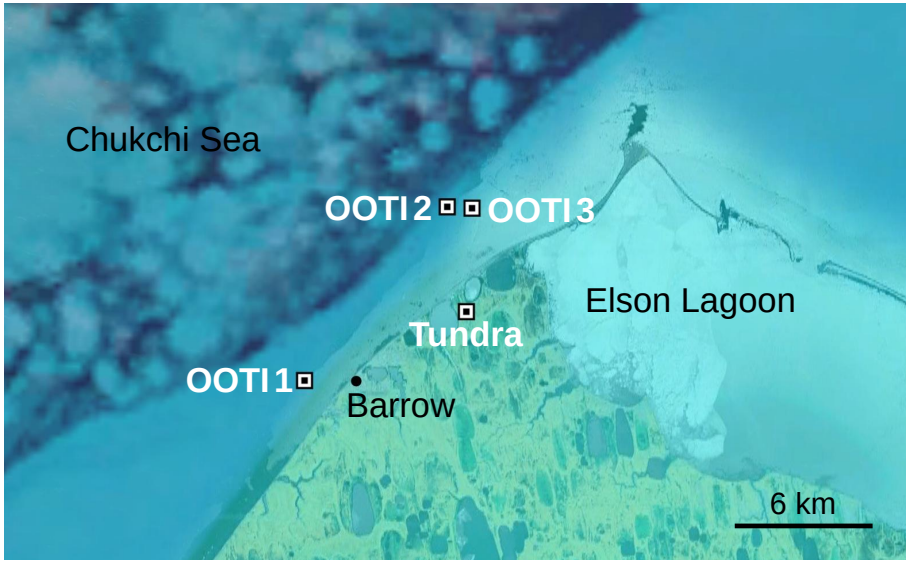

Fig. 1a. Field experimental sites around Barrow near the northernmost tip of Alaska. OOTI 1 at 71.29° N; 156.85° W, OOTI 2 at 71.36° N; 156.69° W, OOTI 3 at 71.36° N; 156.66° W, and Tundra at 71.32° N; 156.66° W. The MODIS Aqua satellite is translucently overlain to show sea ice conditions in the Chukchi Sea on 19 March 2009.

ACPD
13, 5687–5728, 2013

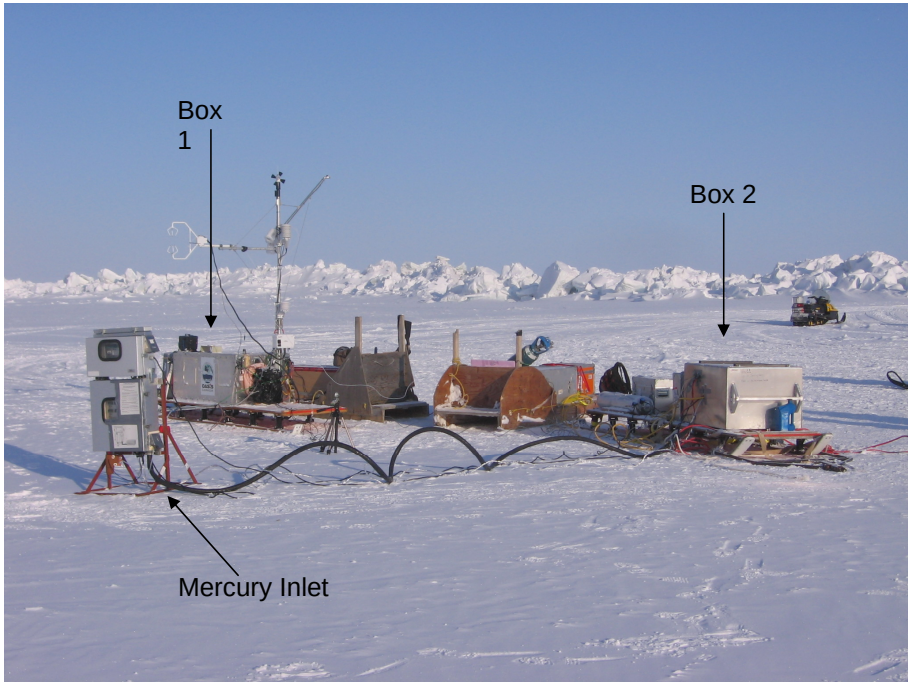

Fig. 1b. Experimental set up of the Out On The Ice System. Box 1 housed the meteorological and ozone instrumentation. Box 2 housed the mercury instrumentation. The inlet for the atmospheric mercury measurement is shown.

ACPD
13, 5687–5728, 2013

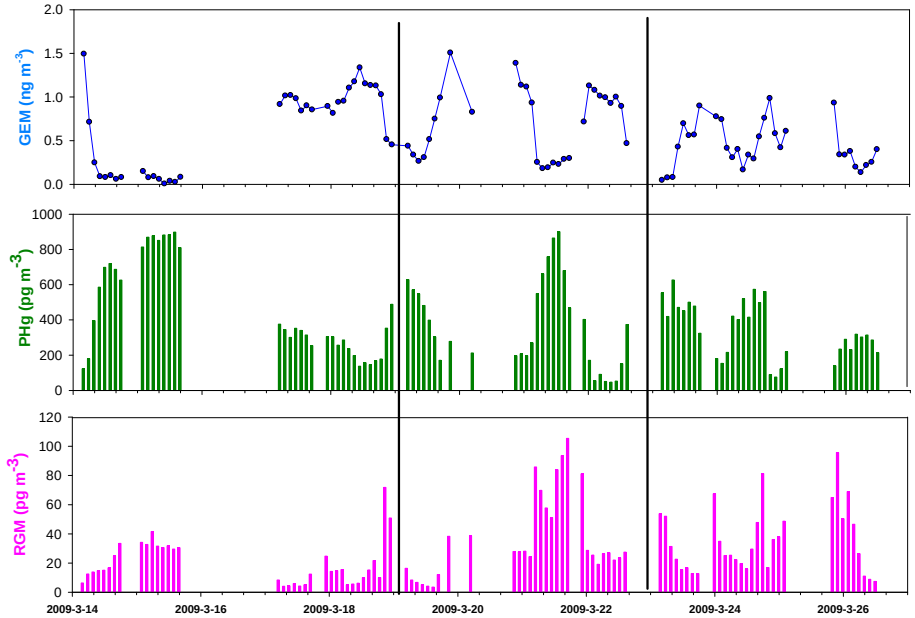

Fig. 2. Hourly speciation data from over the ice. Gaseous elemental mercury (top) is reported in ng m^{-3} and Reactive gaseous mercury (RGM – bottom) and Particulate mercury (PHg – middle) are reported in pg m^{-3}. The gaps in data are when the system was moved to a new site (vertical black lines) or when the power failed.

ACPD
13, 5687–5728, 2013

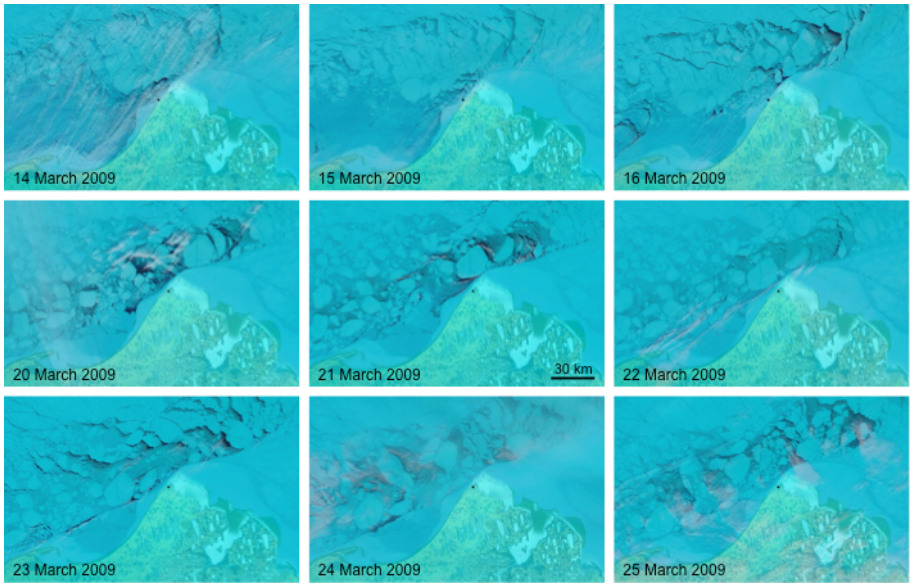

Fig. 3. Modis satellite images of the sea ice Sea ice conditions for 14–25 March 2009. 14–16 March, 20–22 March, and 23–15 March are from when samples were collected over the sea ice at Sites 1, 2 and 3, respectively. 14–16 March represents Event 1; 20, 21 and 24 March represent Event 2 and 25 March represents Event 3. The black dot indicates the sampling location. The colours represent as follows: very light blue (lake ice or ice lagoon); light blue (first-year or older sea ice); darker blue (thinner and younger sea ice) and black (open water or thin new/nilas ice).

ACPD
13, 5687–5728, 2013

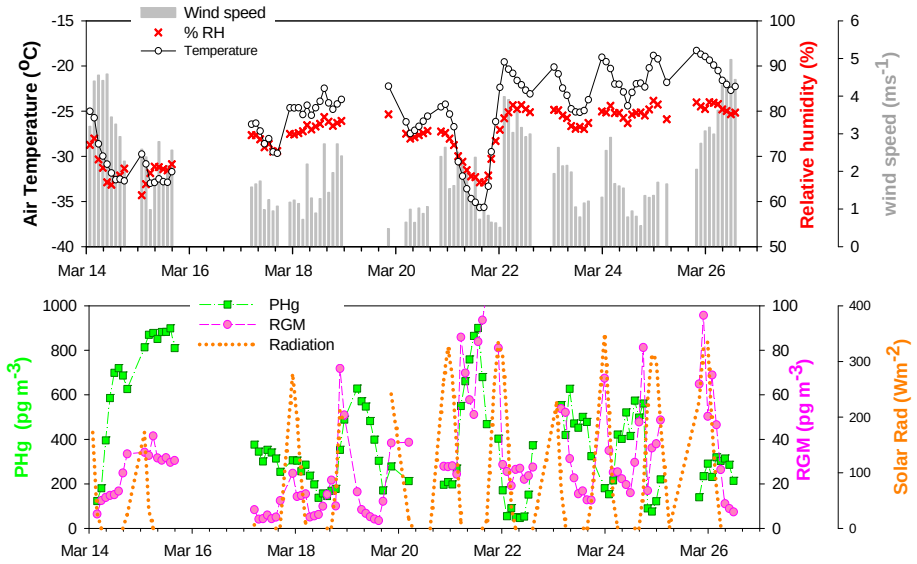

Fig. 4. Meteorological data from on the ice (top panel) and net solar radiation (from tundra site) with RGM and PHg on the ice (bottom panel). Times are in UTC.

ACPD
13, 5687–5728, 2013

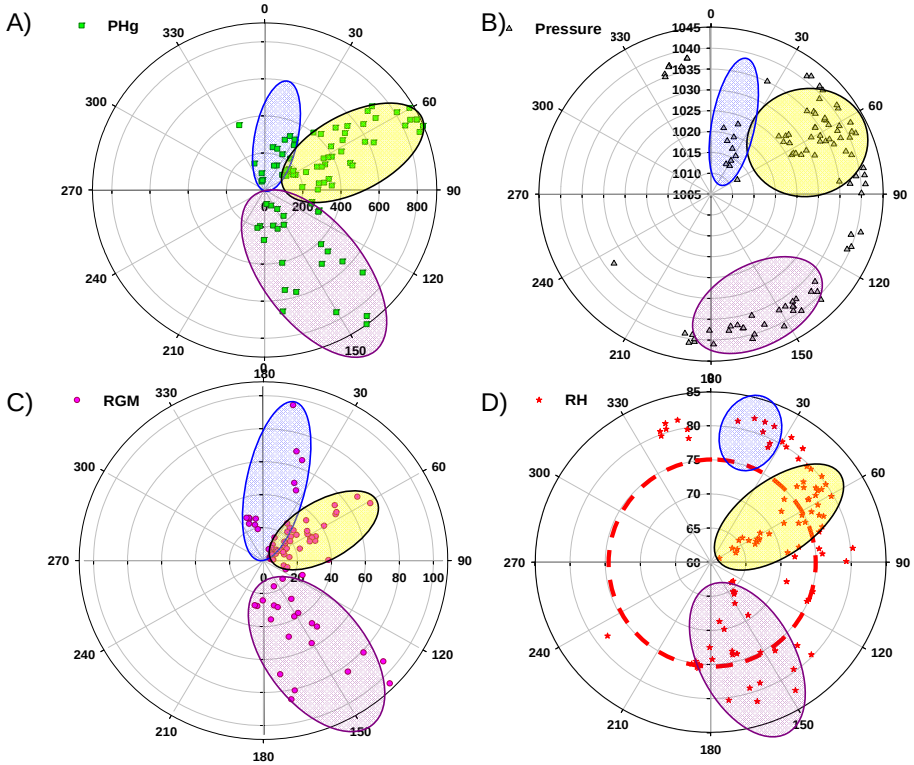

Fig. 5. Wind roses of **(A)** PHg concentration data (pg m^{-3}), **(B)** air pressure (mB), **(C)** RGM concentration data (pg m^{-3}) and **(D)** percent relative humidity (%) for the data from 14–27 March 2009 from over the sea ice.

ACPD
13, 5687–5728, 2013

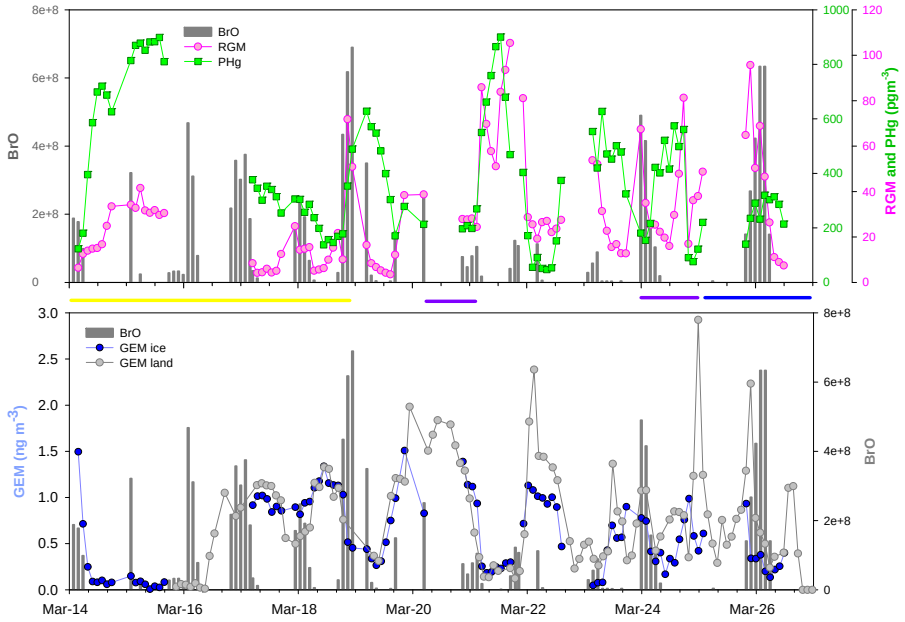

Fig. 6. BrO and PHg/RGM measurements over the sea ice and BrO and GEM measurements over both tundra and sea ice. Events 1, 2 and 3 are marked as yellow, purple and blue, respectively.

ACPD
13, 5687–5728, 2013

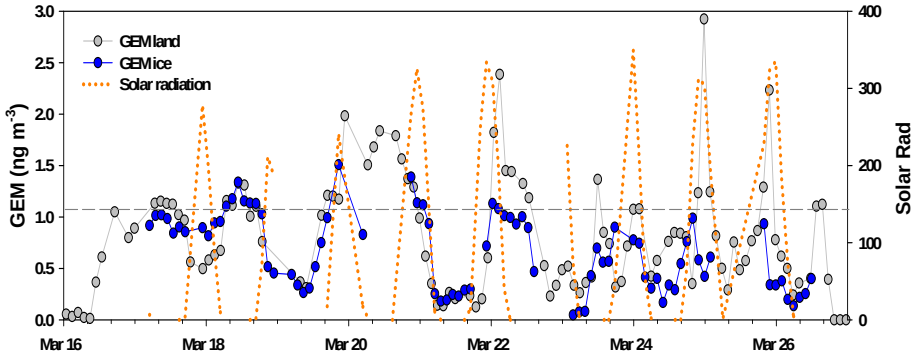

Fig. 7. GEM measurements over tundra inland (grey circles), over the sea ice (blue circles), solar radiation (dark blue) and the defined threshold for mercury depletions (1.063 ng m^{-3}) (dashed grey line).

ACPD
13, 5687–5728, 2013

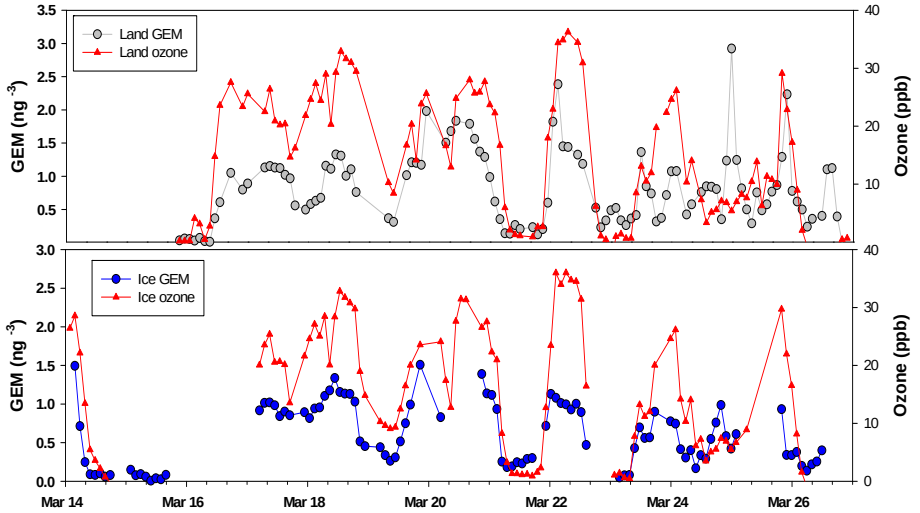

Fig. 8. Hourly averaged GEM (ng m^{-3}) and ozone (ppb) over tundra and sea ice.

ACPD
13, 5687–5728, 2013